Journal of Polymers and the Environment (2020) 28:100–115
https://doi.org/10.1007/s10924-019-01592-y

ORIGINAL PAPER

Enhancing the Thermal, Mechanical and Swelling Properties of PVA/Starch Nanocomposite Membranes Incorporating g-C_3N_4

Arooj Ahmed[1] · Muhammad Bilal Khan Niazi[1] · Zaib Jahan[1] · Ghufrana Samin[2] · Erum Pervaiz[1] · Arshad Hussain[1] · Muhammad Taqi Mehran[1]

Published online: 25 October 2019

Abstract

A ground-breaking and soft nanomaterial, namely graphitic carbon nitride (g-C_3N_4) has gained importance as two-dimensional filler in polymeric membranes. In this research, g-C_3N_4 was synthesized by "thermal oxidation etching process", employing melamine as a precursor. The porous nanosheets were characterized by SEM, XRD and FTIR. g-C_3N_4 nanosheets showed remarkable thermal stability up to 620 °C. The PVA starch nanocomposite membranes were fabricated with varying amounts of g-C_3N_4. Owing to strong interactions between g-C_3N_4, and polymers, the composite membranes showed exceptional thermal and mechanical stability and resist to degrade in various mediums including water, saline and blood. The hybrid membranes showed remarkable swelling abilities up to 96 h. Moreover, g-C_3N_4 enhanced the hydrophilicity, consequently, moisture retention capability and water vapor transmission were improved. XRD and SEM results revealed the proper dispersion of g-C_3N_4 into the polymeric matrix. The results suggested that prepared hybrid PVA/St/g-C_3N_4 membranes could be used as wound dressings.

Graphic Abstract

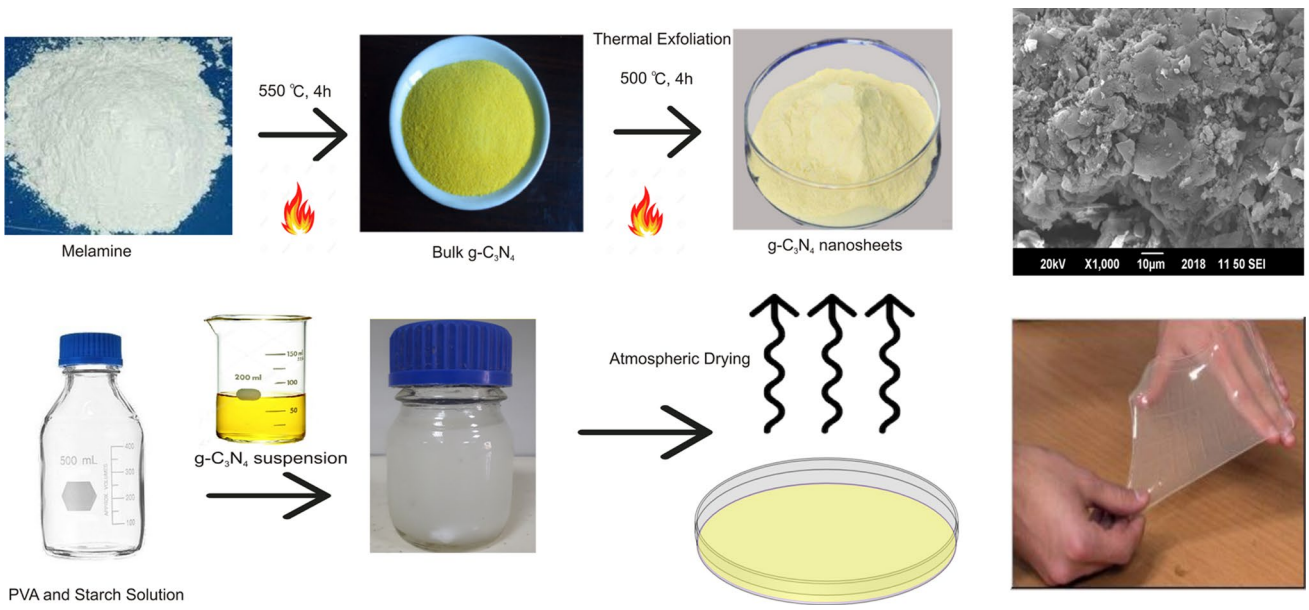

Keywords Membranes · PVA · Starch · g-C3N4 · Swelling · Hydrophilic · Nanocomposite

✉ Muhammad Bilal Khan Niazi
m.b.k.niazi@scme.nust.edu.pk

Extended author information available on the last page of the article

Introduction

Membrane technology is one of the emerging technologies that the world has witnessed during the last few decades [1]. The reason for this emergence is certain advantages of membrane systems over their conventional counterparts. Some of these benefits are simplicity [2], compactness, low energy consumption, easy to up and down scale [3], economical and compatible with the environment regulations [4, 5]. Broadly, membranes are classified as biological and synthetic [6]. Among them synthetic membranes have been the focus of researchers due to their tunable properties. Synthetic membranes can be organic (polymeric) or inorganic (ceramic) in nature.

Polymeric membranes are less costly and offer better control of desirable properties as compared to inorganic membranes [7]. Furthermore, their film formation is easy and simple, and they can selectively transfer the chemical species. The increase in their popularity is due to the wide range of applications. They have been extensively applied in food, chemical, pharmaceutical [8], gas separations [9], aromatherapy [10], membrane distillation [11], drug delivery [12], membrane bioreactors (MBR) [13], biomedical applications ranging from artificial cells to active surfaces [14] and countless others. Various polymers for instance cellulose [15], poly ether sulfone [16], polyamide [17], polymethyl methacrylate (PMMA) [18], polyvinyl pyrrolidone (PVP) [19], poly 2-hydroxy ethyl methacrylate (HEMA) [20] etc. are exploited to use in different areas. Unfortunately, some disadvantages are associated with the polymeric membranes that limit their application like prone to fouling, low flux, poor mechanical strength, low thermal and barrier characteristics [7].

Poly vinyl alcohol (PVA) is a synthetic and water soluble polymer [21]. It is biocompatible, biodegradable, nontoxic, noncarcinogenic and inexpensive polymer [22]. Owing to its excellent film forming ability, less susceptibility to fouling, thermal confrontation, transparency, processability and capability to retain enough water [23], it has found applications in contact lenses [24], drug delivery [25], superabsorbent [26], artificial organs [27], gas separations [28], hardening of cement composites [29], food packaging [30], fuel cells [31] etc. Limited hydrophilicity [32] and dimensional instability [33] of PVA restricts its alone usage in few applications. To overcome this issue, it has been blended with natural polymers especially polysaccharides [34]. They have been observed to produce flexible, economical and effective membranes. PVA and Starch (St) have good compatibility [35]. Starch can be obtained from rice, wheat, potato and corn [36]. It is composed of 30% amylose and 70% amylopectin [37], a linear and a highly branched structure, respectively. PVA and starch are cross linked either by physical or chemical methods. Freeze-thawing (FT) cycles and lyophilization are physical crosslinking method but they are time and energy consuming [38]. Instead, chemical agents for example borax [21], carbodiimide [39], boric acid [40], epichlorohydrin [41], genipin [42] etc. are employed. Glutaraldehyde (GA) has been preferred because of its ability to support intermolecular reaction with PVA and absence of any thermal treatment required to initiative the reaction [43]. The objective of crosslinking is to enhance the mechanical stability of polymeric structure. To alter the physical properties of the membrane, plasticizers are incorporated to induce elasticity and flexibility [44]. They are nontoxic and have low molecular weight [45]. Commonly used plasticizers are poly ethylene glycol (PEG), glycerol, sorbitol etc.[46].

Inorganic compounds have upright mechanical properties, are more resistant to chemical and thermal attacks and can tolerate extreme conditions (pH, corrosive solvents, temperature etc.) [47]. Inorganic, environment friendly and nontoxic graphitic carbon nitride (g-C_3N_4) has been the subject of keenness. Its high thermal and chemical stability, lamellar structure, good mechanical strength and low manufacturing cost render it the most suitable filler for the polymeric membranes [48]. Other inorganic fillers such as zeolite immedazolite framework (ZIF) [49], Fe_3O_4 [50], silica [51], carbon nanotubes [52] etc. are reported in the literature.

Keeping this in mind, an organic–inorganic hybrid membrane was fabricated by the solution casting technique. PVA/St entailed the polymeric matrix and g-C_3N_4 was incorporated as reinforcement. g-C_3N_4 was prepared by thermal condensation technique, using melamine as a precursor. Fourier Transform Infrared Spectroscopy (FTIR) was conducted to investigate the interaction of functional groups. Scanning Electron Microscopy (SEM) provided insight of the morphology of membranes. Phase identification was done by X-ray diffraction (XRD). Physical properties including tensile testing, moisture retention, equilibrium swelling ratio (ESR), water vapor transmission rate (WVTR), porosity and oxygen permeability were evaluated. The crosslinking efficiency was evaluated by gel fraction.

Methods and Materials

Materials

Poly (vinyl alcohol) (PVA, degree of polymerization = 1500, average molecular weight = 30,000–70,000 Da and 87–90% hydrolyzed), starch, glutaraldehyde (50% aqueous solution), ethanol (97 wt%), hydrochloric acid (31% aqueous solution) and glycerin were supplied by Daejung Korea. Sulfuric acid (95–97%) was purchased from Scharlau Spain. Sodium

thiosulfate ($Na_2S_2O_3$) and Sodium Hydroxide (NaOH) were obtained from Merck Germany. Potassium Iodide (KI), Sodium Chloride (NaCl) and Magnesium Chloride ($MgCl_2$) were acquired from Ridel-de-Haen. Melamine (99%), Manganese Sulfate and Sodium Azide were bought from Sigma Aldrich USA. All the reagents were of analytical grade and used as received. Distilled water was used throughout for synthesis purpose.

Synthesis of g-C3N4

The bulk g-C_3N_4 was synthesized by the method reported in literature [53]. Briefly, 3 g of melamine was placed in alumina crucible and was heated to 550 °C at a heating rate of 5 °C/min in a box furnace for 4 h. Then, it was allowed to cool to ambient temperature (30 °C). After calcination, the yellow colored cluster was obtained that was ground to fine powder in pestle and mortar. The thermal exfoliation was carried out by heating bulk g-C_3N_4 to 500 °C at heating rate of 10 °C/min Again it was cooled to room temperature. The obtained light yellow powered was dispersed in water and ethanol solution in 3:1, and ultrasonicated for 6 h. The resulting mixture was centrifuged and dried.

Fabrication of Membranes

The membranes were prepared by the method adopted from Awais Hassan et al. with slight modifications [54]. 5 g PVA was dissolved in 35 ml of water with continuous stirring at 90 °C for 3 h. Furthermore, 3.5 g starch was dissolved in 35 ml water under continuous stirring at 110 °C for 20 min. Starch solution was cooled and then mixed with PVA. Different amount of g-C_3N_4 were dispersed in 10 ml water by carrying out sonication for 40 min. g-C_3N_4 suspension was then poured into homogenous polymer (PVA/St) solution. To prepare GA crosslinking reagent, 0.5 ml GA was mixed with 0.05 ml HCl and 10 ml ethanol. Then it was added to solution with continual stirring. Finally, 2 ml of glycerin was added and stirred for another 30 min to ensure proper mixing. The resultant solution was then casted into glass petri dishes and were left atmospheric drying for 48 h. The membranes were removed from petri dishes and stored in air tight bags.

During the cross linking of polyvinyl alcohol with glutaraldehyde, inter and intra molecular forces of hydrogen bonding takes place that would lead to acetal formation. A condensation reaction between PVA and GA takes place with the elimination reaction of small molecules i.e. (H_2O) as shown in Fig. 1 [55].

The glutaraldehyde (GA) molecules linked the starch chains, during the cross linking the C=O double bonds are opened up and the linkages occurred between the reactive C-6 hydroxyl groups of starch and the glutaraldehyde hydrated regions as shown in Fig. 1.

The addition of PVA to the starch cross linked by glutaraldehyde, the abundant –OH groups of PVA are linked in conjugation through predominant hydrogen bonding with the –OH groups present in Starch and as a result the crosslinking occurs between PVA and starch [56].

The nanofiller Graphitic carbon nitride (g-C_3N_4) surface functional groups (–NH_2, –NH etc.), forms H-bonding with –OH groups of starch as well as PVA –OH groups, thus interactions of starch and PVA with g-C_3N_4 occurs as a result of strong intermolecular forces of hydrogen bonding as shown in Fig. 2. The predominant interaction between nano filler and polymer matrix is hydrogen bonding, besides which Van der waals forces and dipole- dipole interactions are also present between these polar molecules of polyvinyl alcohol, starch and graphitic carbon nitride. These interactions lead to a good dispersion of nano filler in starch and PVA matrix during membrane fabrication [57, 58].

X-ray Diffraction (XRD)

The X-ray Diffraction (STOE-Germany) was used to investigate the crystalline nature of g-C_3N_4 and membranes. The voltage and current of X-ray source were 40 kV and 40 mA, respectively. The samples were scanned at a step size of 0.04, step time of 0.5 s/step and 2θ ranged from 10° to 45°. The wavelength of CuKα radiation was 1.540 Å. The d-spacing was evaluated by Bragg's law [59]:

$$d = \frac{n\lambda}{2\sin\theta} \quad (1)$$

where n is order of reflection, λ is wavelength of X-rays, d is the characteristic spacing between crystal planes of a given specimen and θ is the angle formed between incident beam and that normal to the lattice plane.

Fourier Transform Infrared Spectroscopy (FTIR)

FTIR was used to study the interfacial interactions in the membranes employing Attenuated Total Reflectance, Fourier Transform Infrared Spectroscopy (ATR-FTIR, BRUKER). The analysis was carried out in the range of 4000–500 cm^{-1} at resolution of 4 cm^{-1} and scanning frequency of 32.

Scanning Electron Microscopy (SEM)

The morphology of g-C_3N_4 and membranes were recognized by SEM (JSM-64900). Prior to analysis, a thin conductive layer of palladium/platinum was used to cover the samples. The cross-section of membranes was also analyzed.

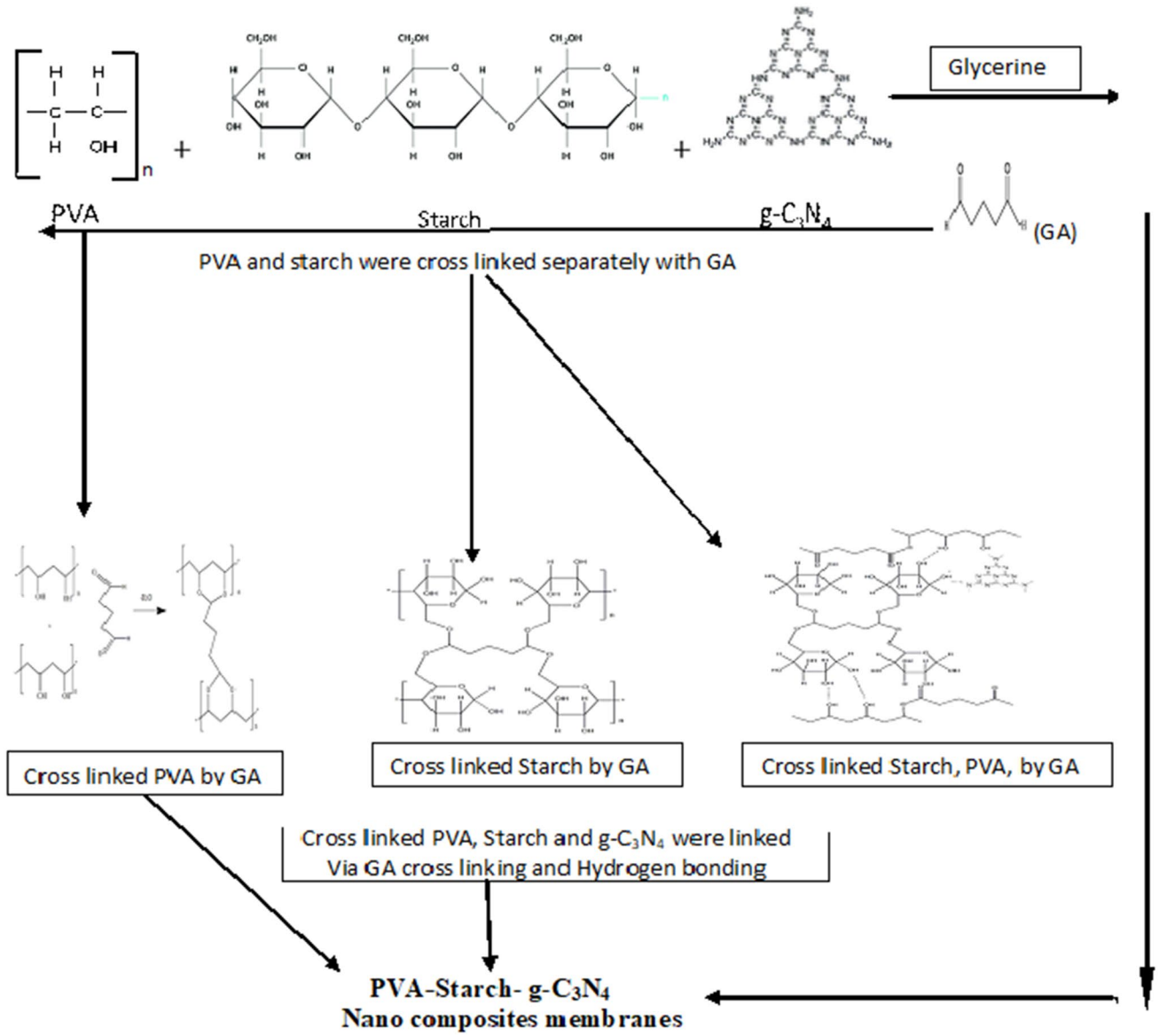

Fig. 1 Schematic depiction illustrating the synthetic route of PVA-Starch-g-C_3N_4 nano composites membrane

Thermal Gravimetric Analysis (TGA)

Thermal Gravimetric Analysis of g-C_3N_4 and nanocomposite membranes was carried out in the temperature range of 20–700 °C in a nitrogen atmosphere at a gas flow of 50 ml/min.

Mechanical Properties

To analyze the mechanical properties of prepared membranes, tensile strength (TS) and elongation at break (EB) were measured. Trapezium-X Universal Testing Machine (AG-20RRKNXD Plus) manufactured by Shimadzu corporation was used for this purpose. According to ASTM D882 standard, the membranes were cut into rectangular pieces of 60 mm × 10 mm dimension. The test was conducted at a crosshead speed of 10 mm/min under 20 kN load cell. The thickness and gauge length of the samples was 0.63 mm ± 0.05 mm and 50 mm, respectively. All studies were carried out five times.

Gel Fraction

To carry out gel fraction (GF) study, the membranes were cut into 10×10 mm^2. After weighing them initially, all samples were placed in oven until a constant weight was acquired. The weight was recorded as W_1. Then, they were immersed in distilled water for 4 consecutive days. After

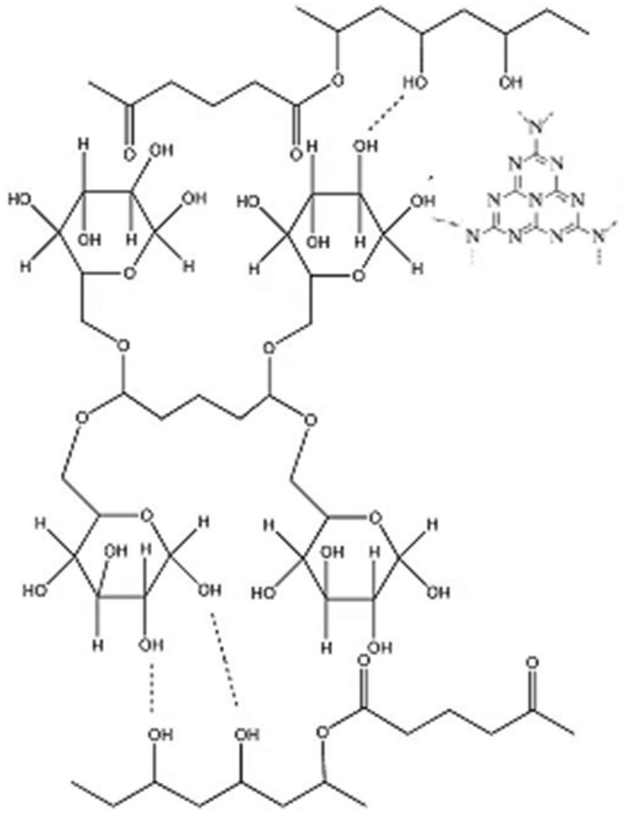

Fig. 2 Cross linked membrane of PVA, Starch and g-C_3N_4 via GA through hydrogen bonding

4 days, the samples were taken out and again placed in oven until a constant weight was attained. This weight was recorded as W_2. The GF was calculated by the formula [60]:

$$\text{Gel fraction } (\%) = \frac{W_2}{W_1} \times 100 \tag{2}$$

The test was performed in triplet to minimize error.

Moisture Retention Ability

The specimen was cut into equal size and weighed initially, denoted as W_1. The membranes were placed in oven at 40 °C for 6 h. After the mentioned time, the samples were taken out of the oven and were weighed again, denoted as W_2. The moisture retention was calculated by the formula [61]:

$$\text{Moisture retention ability } (\%) = \frac{W_2}{W_1} \times 100 \tag{3}$$

Water Vapor Transmission Rate (WVTR)

WVTR studies were performed according to European Pharmacopeia (EP) standard [22]. The round bottles of known diameter were filled with 10 ml deionized water and samples were fixed onto them. To ensure accuracy, the mouth was sealed by means of Teflon tape. The initial weight was recorded as W_1. Then, they were placed in oven at 40 °C for 24 h (t). After 24 h, the bottle was taken out and its weight was recorded as W_2. The open and closed bottles served as negative and positive control, respectively. WVTR was found by following formula:

$$\text{WVTR } \left(\text{g/m}^2\text{h}\right) = \frac{(W_1 - W_{2)}}{Axt} \tag{4}$$

where A is the permeation area of membranes, m2.

Swelling Behavior

To estimate the swelling ratio, the membranes were cut into equal size and their initial dried weight was noted as W_d. Then, the specimen was immersed in water, blood, saline and 0.9% $MgCl_2$. The pH of these solutions was measured. The samples were taken out after regular interval at 24 h, 48 h, 72 h and 96 h. Their weight was noted as W_s. Swelling ratio was then calculated as [62]:

$$\text{Swelling ratio } (\%) = \frac{(W_s - W_d)}{W_d} \times 100 \tag{5}$$

Porosity

The density and porosity of the prepared membranes was evaluated by Archimedes Rule [63]. Ethanol was used as a displacement fluid. Briefly, a container with known volume of ethanol was weighed (W_1). Then, the sample was weighed (W_s) and immersed in the fluid. After complete saturation of the sample, the container was weighed (W_2) again. Afterwards, the sample was removed from container with care and container was weighed (W_3). Following equations were used to perform calculations:

$$V_s = \frac{W_2 - W_3 - W_s}{\rho_h} \tag{6}$$

$$V_p = \frac{W_1 - W_2 + W_s}{\rho_h} \tag{7}$$

$$\rho_s = \frac{W_s \rho_h}{W_1 - W_2 + W_s} = \frac{W_s}{V_s} \tag{8}$$

$$\in = \frac{W_2 - W_3 - W_s}{W_1 - W_3} = \frac{V_s}{V_p + V_s} \tag{9}$$

where V_s is the volume of the sample (ml), V_p is the volume of the pores (ml), ρ_s is the density of sample (g/ml), ρ_h is the density of ethanol (g/ml) and $\in$ is the porosity of the sample.

Oxygen Permeability

The oxygen permeability was carried out by estimating the dissolved oxygen (DO) in the water. The sample membranes were placed on the top of the bottle containing 200 ml deionized water. The mouth of bottles was sealed with Teflon tape. Then, the bottles were placed at room temperature for 24 h. After 24 h the water was analyzed, and dissolved oxygen was determined according to Winkler's Method [64]. The positive and negative control were an open and a closed container, respectively. The O_2 permeability values were expressed as mg/l.

Results and Discussion

X-ray Diffraction (XRD) Analysis

Figure 3a shows the XRD spectrum of g-C_3N_4. It features two characteristic diffraction peaks. The strong peak found at 27.5° is assigned to the interlayer stacking of conjugated aromatic planes, indexed as (002) with d-spacing of 0.325 nm. In addition, the weak peak at almost 13° (d-spacing = 0.693) is the characteristic of in plane structural packing motif of tri-s-triazine units, indexed as (100) [65, 66]. This indicated the triangular nanopores with the building blocks of tri-s-triazine units. Figure 3b depicts the XRD pattern of fabricated membranes with different formulations. For PVA/St membrane without g-C_3N_4, only one peak is observed at 19.8° (101) plane of PVA. The intensity of this peak increased with the incorporation of g-C_3N_4 nanosheets. The increase in crystallinity may be attributed to the dominance of nucleating effect [67]. Furthermore, an important role is played by the strong interfacial interactions between PVA, g-C_3N_4 and glutaraldehyde, but this effect is less pronounced. The characteristic peak of g-C_3N_4 was undetectable, even at higher concentrations. This depicts the effective exfoliation and homogenous dispersion of nanosheets into the polymer matrix. The XRD analysis exposed the good compatibility of g-C_3N_4 with PVA, St and the added crosslinker. As the amount of g-C_3N_4 was increased to 0.14 g and 0.18 g, the characteristic peak of g-C_3N_4 appeared at 27.62 that indicates that at the said amount the agglomeration has started, and this is also clear from SEM results. The obtained results were in accordance with the ones reported in literature [66].

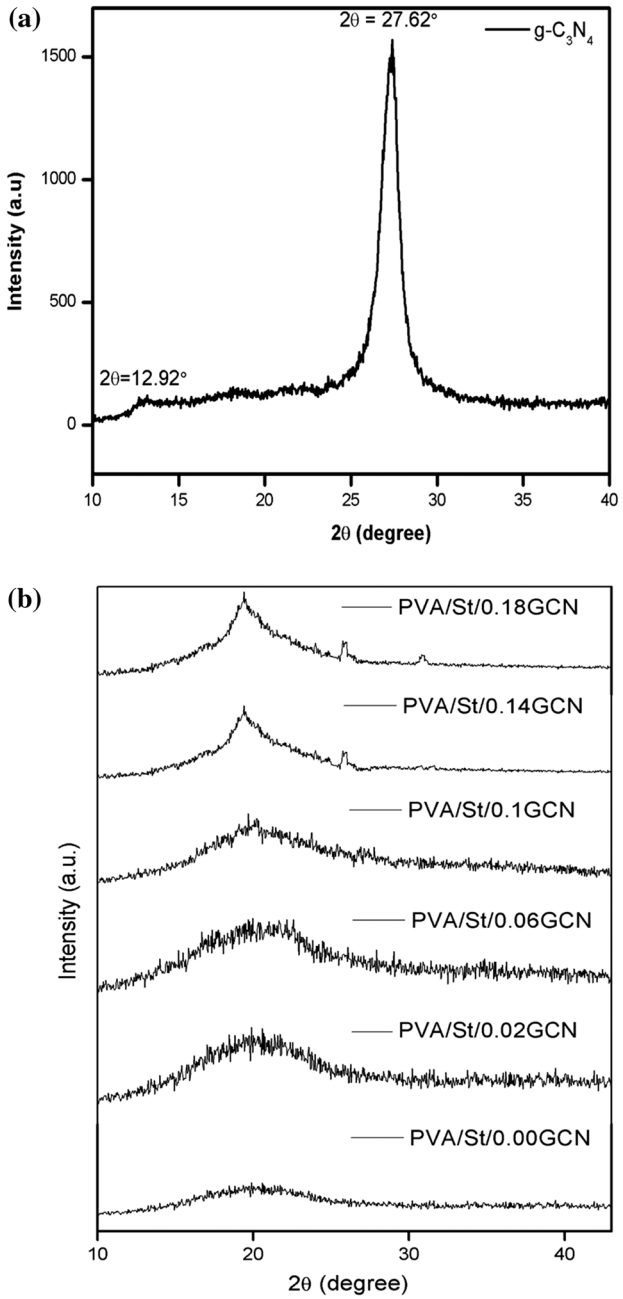

Fig. 3 XRD Pattern of **a** g-C_3N_4 and **b** PVA/St/GCN nanocomposite membranes

Fourier Transform Infrared Spectroscopy (FTIR)

The FTIR spectrum of g-C_3N_4 nanosheets is depicted in Fig. 4a. The peak at 810 cm^{-1} is related to s-triazine ring mode [68]. The distinctive peaks appearing at 1250–1640 cm^{-1} was attributed to the C–NH–C and N–C_3 stretching vibration modes [69]. A broad peak at 3180 cm^{-1} is assigned to stretching modes of primary and secondary amines and intermolecular hydrogen bonds.

Figure 4b indicates the FTIR spectrum of nanocomposite membranes. As the formulations were made from the polymers sharing of similar functional groups, the spectra obtained were quite alike. In case of pure PVA/St membrane (without g-C_3N_4), the peak at 3200 cm^{-1} confirmed the stretching of hydroxyl groups and peak near 2900 cm^{-1} specified sp^3 hybridized hydrocarbon chains (stretching

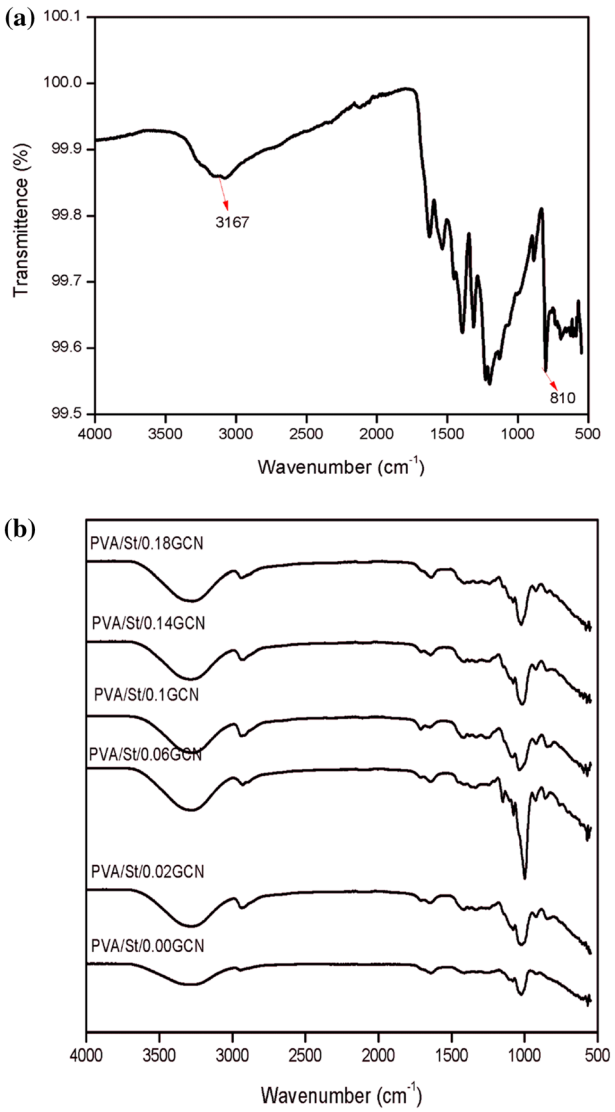

Fig. 4 FTIR spectrum of **a** g-C_3N_4 and **b** PVA/St/GCN nanocomposite membranes

of –CH groups) [70]. When g-C_3N_4 was introduced into the polymeric matrix the characteristic peaks of g-C_3N_4 appeared at 810 cm^{-1} and 1200–1600 cm^{-1}. The peak appearing at 3270–3280 cm^{-1} is due to the presence of hydroxyl groups. The addition of g-C_3N_4 caused a little variation in intensity of stretching of hydroxyl groups. The peak shifting and decrease in relative intensity suggested the formation of strong interfacial interactions between residual –NH or $–NH_2$ of g-C_3N_4 and –OH groups of PVA and Starch that arises due to the hydrogen bonding. The strong band near 1150 cm^{-1} appeared as a result of intra and intermolecular interactions of hydroxyl groups. A band at 1095 cm^{-1} is due to the crosslinking reaction between PVA and glutaraldehyde (C–O–C) group. The absorption band at 1740 cm^{-1} is attributed to stretching of unreacted aldehyde group present in glutaraldehyde [43].

Scanning Electron Micrographs (SEM)

SEM is a promising technique for topographical analysis of the specimens. It provides valuable information about size and shape of the material used [71]. Figure 5a displays the scanning electron micrograph of g-C_3N_4 nanosheets. The result was quite similar to graphene like crenelated two-dimensional morphology of g-C_3N_4 nanosheets. Its ultrafine structure was also confirmed [48].

The morphology of formulated membranes is depicted in Fig. 5b–g. The surface of the membranes was dense, and no visible pores were found, even at higher magnifications. As anticipated, a smooth and homogenous surface for pure PVA and starch was obtained. This indicated the miscibility of components with each other, as presented in Fig. 3b. Similar results have been reported in literature [72]. The smooth surface of PVA/St/g-C_3N_4 composite membrane designated that the addition of crosslinker, GA, not only favored the network formation with polymers but also permitted an effective dispersion of g-C_3N_4. Furthermore, the proper dispersion might be the result of ultrasonication [48]. As the g-C_3N_4 content was increased, partial agglomeration of nanosheets was seen on the surface of PVA/St/0.14GCN hybrid (Fig. 5f) and it became more noticeable in PV0A/St/0.18GCN (Fig. 5g).

To gain further insight of the membranes, cross-section micrographs are shown in Fig. 5h–m. No pores were found for pure PVA/St blend. Furthermore, smooth morphology is observed. However, PVA/St/ g-C_3N_4 formulations have shown pores. g-C_3N_4 was dispersed into the polymetric matrix. The preferential orientation of 2D fillers is parallel to the membrane surface [73] and was observed here too. Moreover, no cracks or defects were observed. The alignment of g-C_3N_4 was disturbed at higher content. This can be attributed to the surface activation energy. It compelled adjacent nanosheets to restack together into agglomerates [74, 75].

Thermal Gravimetric Analysis (TGA)

Figure 6a illustrates the TGA curve for g-C_3N_4. The result demonstrated its unique behavior. g-C_3N_4 is thermally stable up to 620 °C. Therefore, it is suitable to be applied at normal and even high temperatures. According to the studies reported to date, g-C_3N_4 is the most stable allotrope of carbon nitride [48].

The TGA for PVA/St and different formulations of PVA/St/GCN is also analyzed and shown in Fig. 6b. In these curves, three different regions can be observed. The initial weight loss at 70–200 °C is because of the solvent release absorbed by the polymer and loss of

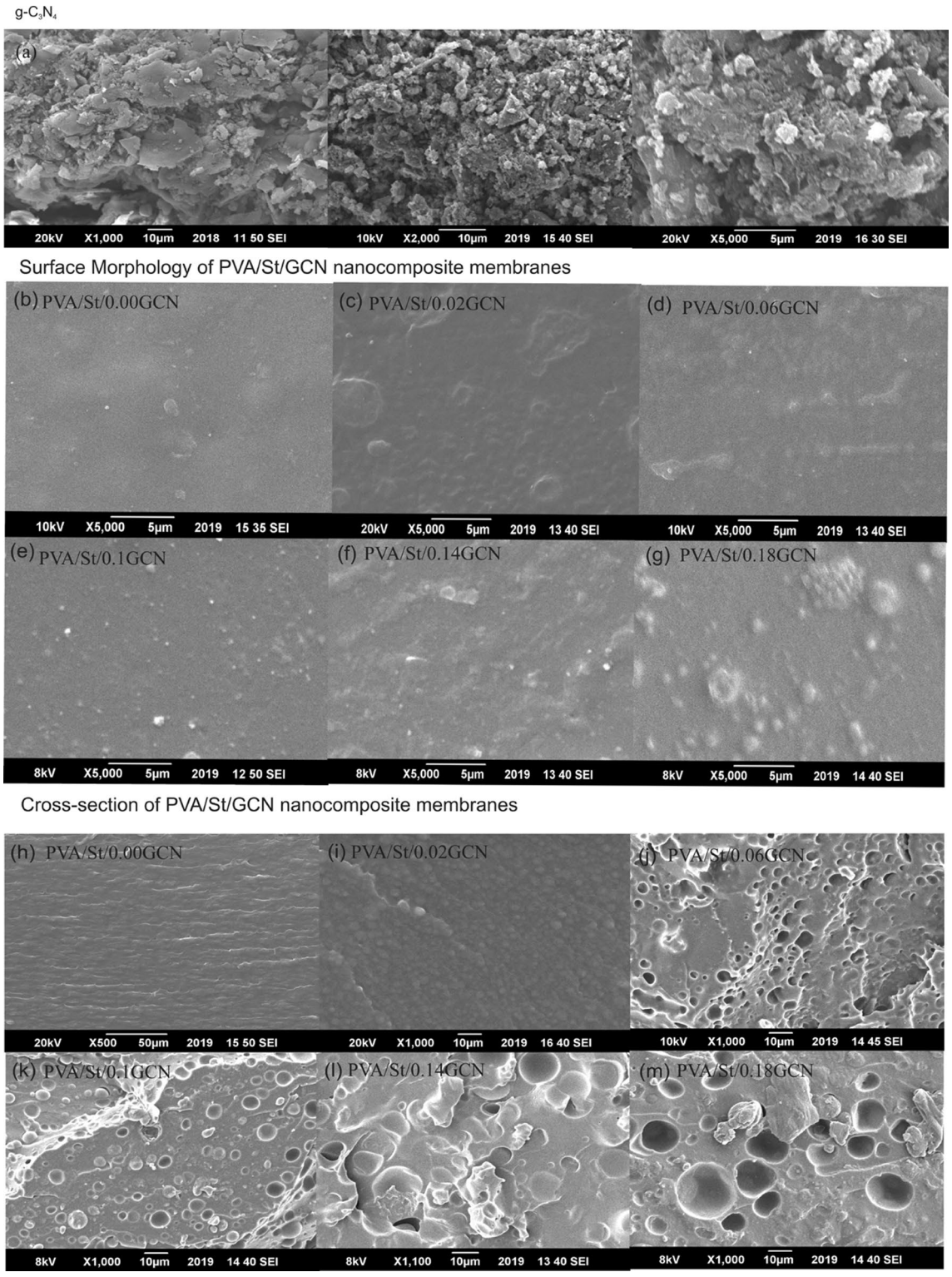

Fig. 5 SEM images of **a** g-C_3N_4, surface morphology of PVA/St, **b** 0.00 g GCN, **c** 0.02 g GCN, **d** 0.06 g GCN, **e** 0.1 g GCN, **f** 0.14 g GCN, **g** 0.18 g GCN and cross-section of PVA/St, **h** 0.00 g GCN, **i** 0.02 g GCN, **j** 0.06 g GCN, **k** 0.1 g GCN, **l** 0.14 g GCN, **m** 0.18 g GCN

volatile matter (e.g. water and glycerin). In the subsequent stage, the degradation of starch and PVA occurs. This is chiefly on account of dehydration of hydroxyl groups and followed by the formation of other carbon species. At this stage, oxygen functional groups are removed, and

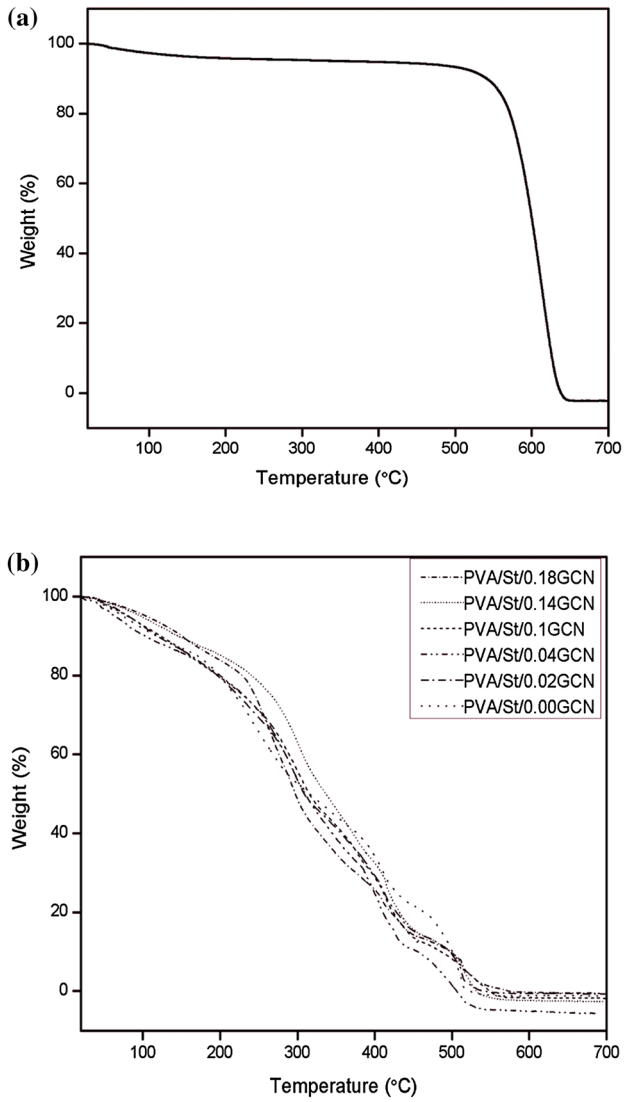

Fig. 6 TGA Curve of **a** g-C_3N_4 and **b** PVA/St/GCN nanocomposite membranes

polyene intermediates are formed. Commonly, scission and decomposition of PVA chains occurs at a temperature above 400 °C. A monotonic decrease in weight is observed until the complete degradation of PVA (almost 240 °C). Starch is more thermally stable as compared to PVA, owing to the presence of cyclic hemiacetal structures in it [72]. Carbonization occurs at last stage, from 500 to 700 °C. It is corresponded to the backbone degradation of crosslinked PVA and starch. Studies have been reported indicating the shift of degradation temperature from 250 to 350 °C [38]. It evidences that crosslinking plays a vital role in enhancing the thermal stability. The results thus obtained confirms the thermal stability of nanocomposite membranes up to 280 °C.

Mechanical Properties

One of the key advantages of incorporating inorganic fillers with polymeric membranes are to improve their mechanical properties and this was fully utilized here. The tensile testing further confirmed the interfacial interactions between polymers and g-C_3N_4. With the increase in g-C_3N_4 amount from 0.02 to 0.14 g, the tensile strength also enhanced, compared with pure PVA/St membranes. The increase in strength was credited to the homogenous dispersion of g-C_3N_4 and strong interfacial interactions between g-C_3N_4 and GA [74, 76]. The improvement in tensile strength was also result of hydrogen bonding. The tensile strength decreased when g-C_3N_4 was further increased to 0.18 g. This was attributed to the deterioration of lamellar structure due to the accumulation of g-C_3N_4 nanosheets [76]. It should be worth noticing that the mechanical strength was still much higher than the pure PVA/St membrane. The results are shown in Fig. 7a.

The results of elongation at break are shown in Fig. 7b and were accordance to literature [60, 77]. The elongation at break decreased gradually with increasing g-C_3N_4 content, the results can be recognized as the addition of g-C_3N_4 into polymeric matrix might accelerate and undermine the break elongation of the membrane. Besides, high g-C_3N_4 might upsurge the hydrophilic susceptibility and decrease the entanglement degree which resulted in reduction of flexibility. The high crosslinking density was also responsible for this behavior. Furthermore, the hardness and brittleness of the membranes enhanced with the increase in g-C_3N_4 content. This also leads to the reduction in elongation.

Gel Fraction

Gel fraction (GF) test is performed to quantitatively assess the effectiveness of the crosslinker used. The GF value ranges in 80–86%. There was a slight decrease with the addition of g-C_3N_4. Figure 8a shows that the gel fraction of pure PVA/St to be almost 86%. This was the maximum value attained. This behavior suggests the entanglement of PVA chains [60]. The decrease in gel fraction values with the addition of g-C_3N_4 may be due to the reduction in entanglement reactions [78]. The obtained results demonstrated the effectiveness of glutaraldehyde as a crosslinker for PVA and St membranes. Similarly, the crosslinked membranes showed better mechanical and thermal stability [38].

Moisture Retention Ability

The moisture retention ability demonstrates the water loss from the membranes. Moisture retention ability with respect to g-C_3N_4 content is exhibited in Fig. 8b. No substantial difference in the values was observed. The moisture retention of all the membranes was < 90%. This is credited to

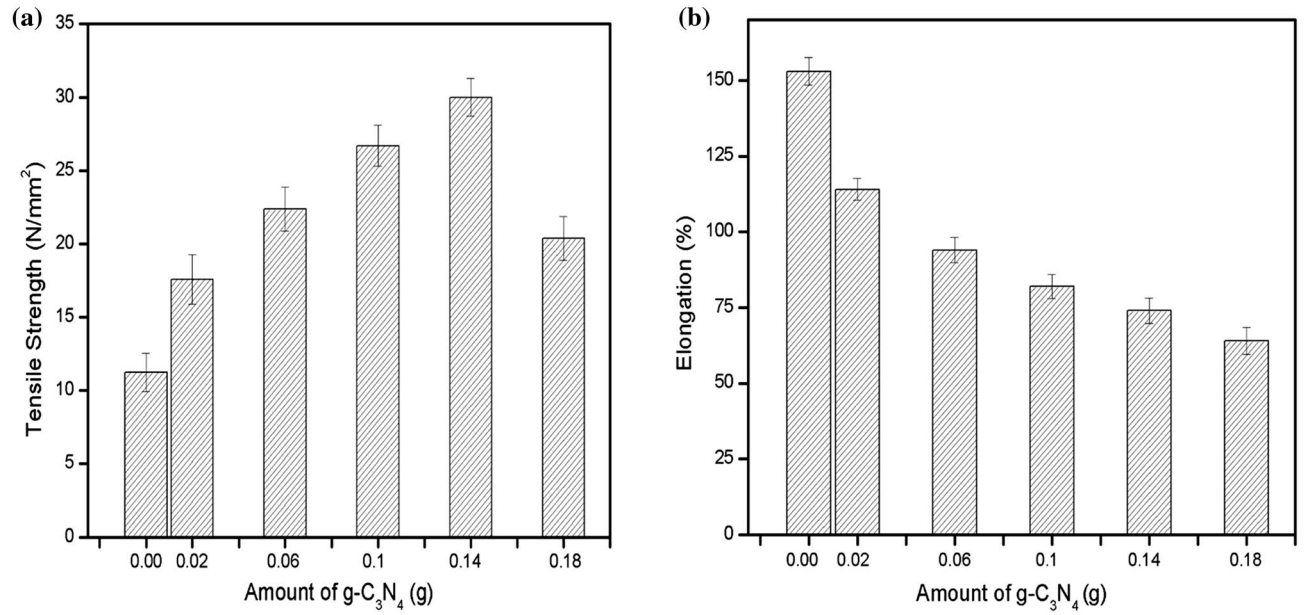

Fig. 7 Mechanical properties **a** tensile strength and **b** elongation at break of PVA/St/GCN nanocomposite membranes

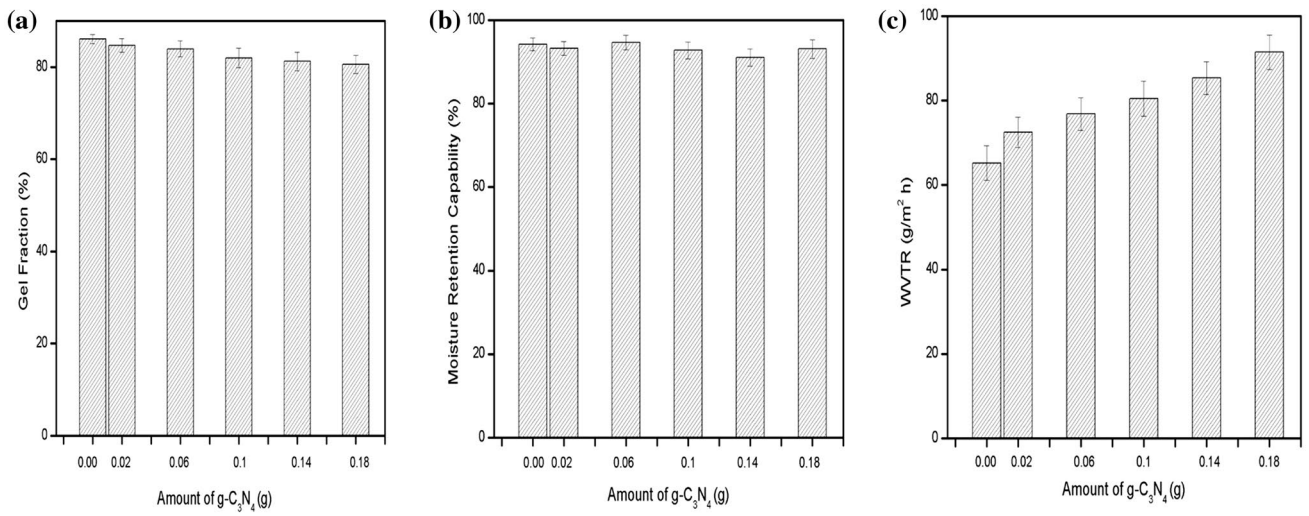

Fig. 8 **a** Gel fraction, **b** moisture retention ability and **c** water vapor transmission rate of PVA/St/GCN nanocomposite membranes

the fact that PVA, Starch and g-C_3N_4 are hydrophilic in nature, thus they can easily combine with the water molecules to form hydrogen bonds [79]. The water gets locked into the robust structure and barely get out of the network. The hydroxyl group (OH) of PVA and St have the ability to absorb and retain considerable amount of moisture [80]. The neutral groups assisted in water retention by contributing in hydrogen bonding [81]. But the higher water retention is not always preferable, all depends on the application. The suggested application of PVA/St/GCN nanocomposite membranes is wound dressings. In that case, high moisture retention values are favored. Because moist bed accelerates the tissue regeneration process [32]. Moreover, in a wet environment the healing of skin takes places without inflammation or eschar formation [82].

Water Vapor Transmission Rate (WVTR)

The WVTR behavior of PVA/St/g-C_3N_4 films is illustrated in Fig. 8c. It was observed that with the rise in amount of g-C_3N_4, the WVTR also increases. The negative and positive controls were a closed and an open bottle, respectively. For the open bottle, the WVTR value was 372.47 g/m^2 h. But the values reduced to a large extent when the bottle was covered

with the membranes. The WVTR of pure PVA/St film is 65.23 g/m^2 h. The WVTRs for PVA/St/0.02GCN, PVA/St/0.06GCN, PVA/St/0.1GCN, PVA/St/0.14GCN and PVA/St/0.18GCN were 72.54, 76.811, 80.47, 85.35 and 91.44 g/m^2h, respectively. The results suggested that the formulated nanocomposite membranes have ability to act as a barrier in preventing the water loss. This again encourage its usage as wound dressings. The increase in WVTR is ascribed to the introduction of hydrophilic g-C_3N_4 [83], having more ability to attract moisture. Moreover, the hydrophilic nature of glycerin also enhanced water permeability through the membranes [84] (Table 1).

Swelling Behavior

Swelling behavior of the formulated membranes was investigated against distilled water, 0.9% NaCl solution, 0.9% $MgCl_2$ solution and blood. A higher degree of swelling was observed for crosslinked PVA films. The factors effecting the swelling are pH, temperature, swelling environment, nature of polymers and degree of crosslinking [71]. The hydrophilic functional groups of g-C_3N_4, PVA and Starch were involved in the swelling of the films. The swelling is affected by the pattern of ionization in the buffer solutions and hydrogen bonding between water molecules [85]. As the crosslinking density decreases, swelling percentage increases [86] and this may be due to reduction in entanglement of polymeric chains. The swelling reached its maximum value in water, as shown in Fig. 9a. In NaCl and $MgCl_2$ solutions, the electrostatic repulsion of ionic charges induced the swelling, that blocks the accumulation of polymer chains and tend to expand the network [87]. With the increase in ionic strength, the osmotic pressure between the polymer network and solution decreased, that delayed the penetration of water molecules into the network of polymer chains [86]. This was the reason for reduction in swelling for NaCl and $MgCl_2$, as shown in Fig. 9b and c. In case of blood (Fig. 9d), the swelling reached its maximum value. This may be ascribed to the fact that crosslinking intensify the molecular spacing between the chains and deteriorate the hydrogen bonding [88]. Moreover, an additional osmotic pressure is created due to the ionic nature of blood that enhances the electroneutrality effect and causes swelling [89].

Table 1 The detailed description for fabrication of PVA/Starch g-C_3N_4 nanocomposite membranes

Membranes	PVA (g)	Starch (g)	g-C_3N_4 (g)	Water (ml)
PVA/St/0GCN	5	3.5	0.00	70
PVA/St/0.02GCN	5	3.5	0.02	80
PVA/St/0.06GCN	5	3.5	0.06	80
PVA/St/0.1GCN	5	3.5	0.1	80
PVA/St/0.14GCN	5	3.5	0.14	80
PVA/St/0.18GCN	5	3.5	0.18	80

Porosity

Porosity more depends on the fabrication process of membrane, rather than the compositions [90]. Archimedes method was selected to determine the density and porosity of membranes, owing to the extensive errors and unsuitable results of other methods [91]. Porosity is the crucial factor as it is responsible for enhancing adsorption and surface area [92]. The rate of solvent diffusion is largely dependent on it. Solvent diffusion is facilitated and aids in interaction with the functional groups present in the network [93]. Furthermore, permeability is also affected by density and porosity. Table 2 enlists the porosity and density of the membranes. For porosity, a decreasing trend is observed with the increase in g-C_3N_4 content. This may be due to the filling of pores, thus making the network more compact but on the cost of consumption of some hydrogen bonds [93, 94]. The porosity was found in the range of 66–75% and highest percentage was found for PVA/St/0.02GCN.

Oxygen Permeability

The obtained results of oxygen permeability are shown in Table 2. The analysis was carried out adopting Winkler's Method and the amount of dissolved oxygen (DO) is measured in water. A divalent manganese solution was added into the flasks followed by the addition of Sodium Hydroxide (NaOH), a strong base. By doing this, DO rapidly oxidized into equal amount of divalent manganese ions (Mn^{2+}) to a higher valency, manganese dioxide, MnO_2 (Mn^{4+}). MnO_2 remained in the form of precipices in the solution. Subsequently, solution was acidified by adding Potassium Iodide. As a result, free iodine ions were produced, that were equal to the actual concentration of oxygen present in receipt water. The water was titrated with sodium thiosulfate solution (0.025 N). Eventually, starch solution was used as an indicator. The endpoint was achieved when the solution turned blue [95]. The dissolved oxygen for open and closed flask was found to be 12.60 ± 3.4 mg/l and 6.00 ± 2.8 mg/l, respectively. Usually, DO in water lies in the range 7 to 14.5 mg/l at 35 °C [96]. For the bottles covered with membranes, the oxygen permeability ranged from 6.91 ± 2.5 to 7.92 ± 3.1 mg/l. The obtained results indicated that adequate amount of oxygen could penetrate into the network and provide sufficient supply of oxygen. Thus, these membranes can be suitable for energy production, tissue engineering and cell repair [97].

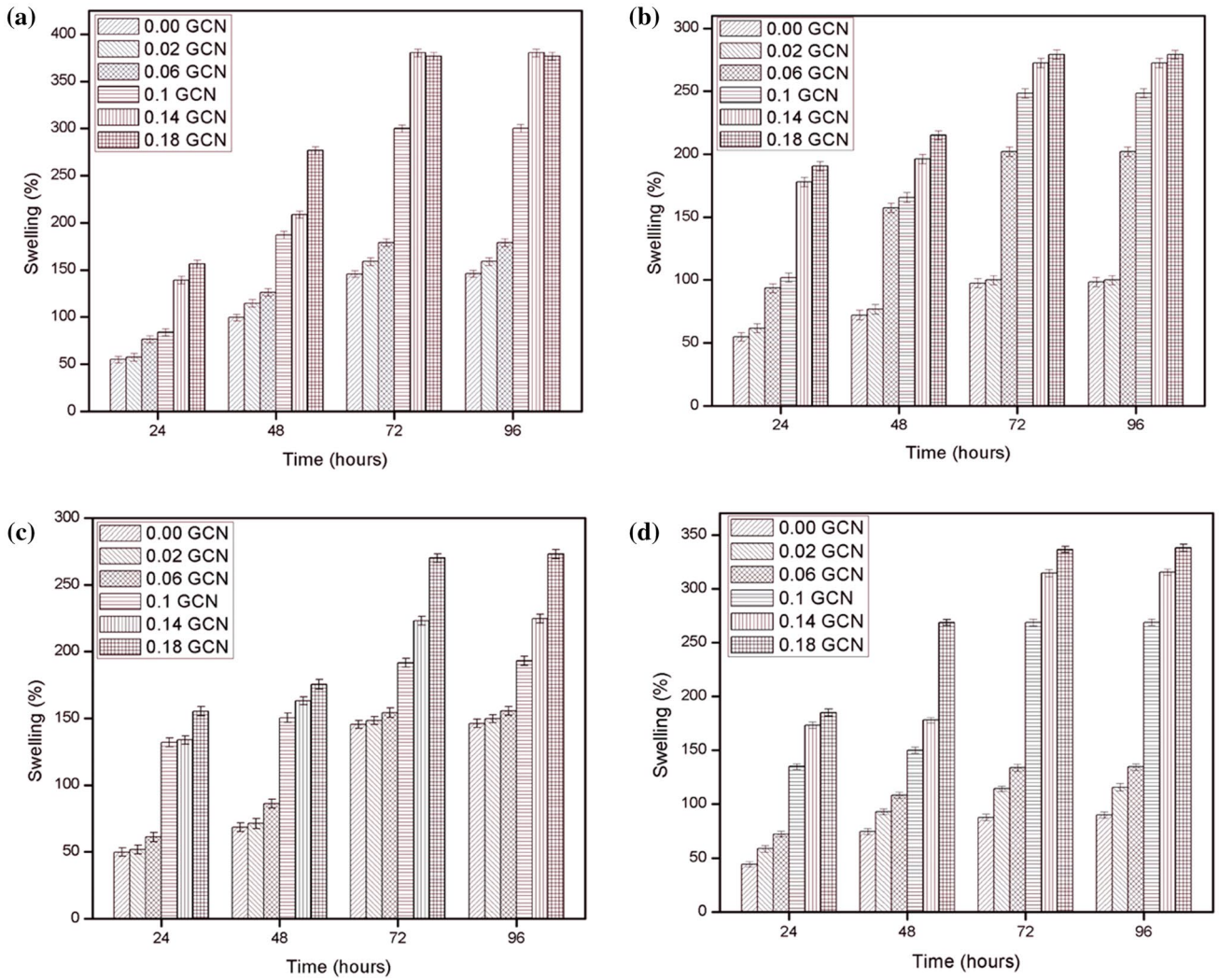

Fig. 9 Swelling behavior of PVA/St/GCN nanocomposite membranes against **a** water, **b** 0.9% NaCl, **c** 0.9% $MgCl_2$, **d** blood

Table 2 Porosity and oxygen permeability of PVA/St/GCN nanocomposite membranes

Amount of g-C_3N_4 (g)	Volume of hydrogel V_g (ml)	Density of hydrogel ρ_g (g/ml)	Volume of ethanol in pores V_p (ml)	Porosity P (%)	Oxygen permeability (mg/l)
0.00	32.34	0.024	60.14	65.02	6.91 ± 2.5
0.02	23.46	0.032	69.46	74.75	7.52 ± 3.1
0.06	26.77	0.028	67.35	71.55	7.92 ± 2.7
0.1	27.55	0.028	65.54	70.40	7.31 ± 2.9
0.14	29.18	0.027	64.46	68.83	7.52 ± 3.3
0.18	31.81	0.027	61.92	66.03	7.92 ± 3.1
Open	–	–	–	–	12.60 ± 3.4
Closed	–	–	–	–	6.00 ± 2.8

Conclusions

In this study, a novel PVA/Starch/g-C_3N_4 nanocomposite membrane was prepared by the solution casting technique. g-C_3N_4 was synthesized by "thermal oxidation etching process". For this purpose, melamine was utilized as a precursor. The polymeric membranes with excellent swelling ability and superior mechanical strength were fabricated by incorporating varying amounts of g-C_3N_4 into the polymeric matrix of PVA and Starch. g-C_3N_4 improved the mechanical properties of the membranes. Incorporation of g-C_3N_4 resulted into its parallel alignment that significantly improved its water barrier properties. The hybrid membranes showed remarkable swelling abilities up to 96 h. FTIR analysis confirmed the hydrogen bonding interactions between NH groups of g-C_3N_4 and OH groups of PVA and starch. The hydrogen bonding resulted into the increase in thermal and mechanical properties. The tensile strength was increased from 11 MPa of pure membrane to 30 MPa for PVA/St/0.14 GCN. The membranes were enough porous to facilitate the adsorption process. The high moisture retention up to 95% was credited to hydrophilicity of PVA, starch and g-C_3N_4. The maximum gel fraction value achieved was 86% that validate the efficiency of crosslinker. Also, it confirms the strong interfacial interactions among PVA, glutaraldehyde and g-C_3N_4. Additionally, the membranes were also permeable to oxygen. The obtained results suggested that g-C_3N_4 has the potential to be utilized as a versatile filler into polymeric membranes. Moreover, these membranes could also be used as wound dressings [22].

References

1. Mulder J (2012) Basic principles of membrane technology. Springer, New York
2. Waheed H, Hussain A (2019) Fabrication of cellulose acetate/polyaziridine blended flat sheet membranes for dialysis application. BioNanoScience 9:1–10
3. Ulbricht M (2006) Advanced functional polymer membranes. Polymer 47(7):2217–2262
4. Dalane K, Dai Z, Mogseth G, Hillestad M, Deng L (2017) Potential applications of membrane separation for subsea natural gas processing: a review. J Nat Gas Sci Eng 39:101–117
5. George G, Bhoria N, AlHallaq S, Abdala A, Mittal V (2016) Polymer membranes for acid gas removal from natural gas. Sep Purif Technol 158:333–356
6. Baker RW (2000) Membrane technology and applications. Wiley, Hoboken
7. Ng LY, Mohammad AW, Leo CP, Hilal N (2013) Polymeric membranes incorporated with metal/metal oxide nanoparticles: a comprehensive review. Desalination 308:15–33
8. Sajitha C, Mohan D (2005) Studies on cellulose acetate-carboxylated polysulfone blend ultrafiltration membranes. III. J Appl Polym Sci 97(3):976–988
9. Favvas EP, Heliopoulos NS, Karousos DS, Devlin E, Papageorgiou SK, Petridis D, Karanikolos GN (2019) Mixed matrix polymeric and carbon hollow fiber membranes with magnetic iron-based nanoparticles and their application in gas mixture separation. Mater Chem Phys 223:220–229
10. Figoli A, Marino T, Galiano F, Blasi E, Belsito E, Liguori A, Leggio A, Rombolà L, Morrone L (2018) Potentiality of polymeric membranes in aromatherapy: application to bergamot essential oil. Sep Purif Technol 207:166–178
11. Lee E-J, Deka BJ, An AK (2019) Reinforced superhydrophobic membrane coated with aerogel-assisted polymeric microspheres for membrane distillation. J Membr Sci 573:570–578
12. Kalita S, Kandimalla R, Devi B, Kalita B, Kalita K, Deka M, Kataki AC, Sharma A, Kotoky J (2017) Dual delivery of chloramphenicol and essential oil by poly-ε-caprolactone–Pluronic nanocapsules to treat MRSA-Candida co-infected chronic burn wounds. RSC Adv. 7(3):1749–1758
13. Ghalamchi L, Aber S, Vatanpour V, Kian M (2019) A novel antibacterial mixed matrixed PES membrane fabricated from embedding aminated Ag3PO4/g-C3N4 nanocomposite for use in the membrane bioreactor. J Ind Eng Chem 70:412–426
14. Garni M, Wehr R, Avsar SY, John C, Palivan C, Meier W (2018) Polymer membranes as templates for bio-applications ranging from artificial cells to active surfaces. Eur Polym J 112:346–364
15. Cheang B, Zydney AL (2004) A two-stage ultrafiltration process for fractionation of whey protein isolate. J Membr Sci 231(1–2):159–167
16. Bhattacharjee S, Bhattacharjee C, Datta S (2006) Studies on the fractionation of β-lactoglobulin from casein whey using ultrafiltration and ion-exchange membrane chromatography. J Membr Sci 275(1–2):141–150
17. Lee SY, Kim HJ, Patel R, Im SJ, Kim JH, Min BR (2007) Silver nanoparticles immobilized on thin film composite polyamide membrane: characterization, nanofiltration, antifouling properties. Polym Adv Technol 18(7):562–568
18. Aroca AS, Ribelles JG, Pradas MM, Garayo AV, Antón JS (2007) Characterisation of macroporous poly (methyl methacrylate) coated with plasma-polymerised poly (2-hydroxyethyl acrylate). Eur Polymer J 43(10):4552–4564
19. Archana D, Singh BK, Dutta J, Dutta P (2015) Chitosan-PVP-nano silver oxide wound dressing: in vitro and in vivo evaluation. Int J Biol Macromol 73:49–57
20. Tomić SL, Mićić MM, Dobić SN, Filipović JM, Suljovrujić EH (2010) Smart poly (2-hydroxyethyl methacrylate/itaconic acid) hydrogels for biomedical application. Radiat Phys Chem 79(5):643–649
21. Han J, Lei T, Wu Q (2013) Facile preparation of mouldable polyvinyl alcohol-borax hydrogels reinforced by well-dispersed cellulose nanoparticles: physical, viscoelastic and mechanical properties. Cellulose 20(6):2947–2958
22. Khorasani MT, Joorabloo A, Moghaddam A, Shamsi H, MansooriMoghadam Z (2018) Incorporation of ZnO nanoparticles into heparinised polyvinyl alcohol/chitosan hydrogels for wound dressing application. Int J Biol Macromol 114:1203–1215
23. Kenawy E-R, Kamoun EA, Eldin MSM, El-Meligy MA (2014) Physically crosslinked poly (vinyl alcohol)-hydroxyethyl starch blend hydrogel membranes: synthesis and characterization for biomedical applications. Arab J Chem 7(3):372–380
24. Hyon S-H, Cha W-I, Ikada Y, Kita M, Ogura Y, Honda Y (1994) Poly (vinyl alcohol) hydrogels as soft contact lens material. J Biomater Sci Polym Ed 5(5):397–406
25. Li JK, Wang N, Wu XS (1998) Poly (vinyl alcohol) nanoparticles prepared by freezing–thawing process for protein/peptide drug delivery. J Control Release 56(1–3):117–126
26. Khoerunnisa F, Hendrawan, Sonjaya Y, Putri OD (2016) Superabsorbent hydrogel composite based on copolymer cellulose/poly

(vinyl alcohol)/CNT. In: AIP Conference Proceedings, vol 1. AIP Publishing, p 020046
27. Chen DH, Leu JC, Huang TC (1994) Transport and hydrolysis of urea in a reactor–separator combining an anion-exchange membrane and immobilized urease. J Chem Technol Biotechnol 61(4):351–357
28. Torstensen JØ, Helberg RM, Deng L, Gregersen ØW, Syverud K (2019) PVA/nanocellulose nanocomposite membranes for CO2 separation from flue gas. Int J Greenhouse Gas Control 81:93–102
29. Arain MF, Wang M, Chen J, Zhang H (2019) Study on PVA fiber surface modification for strain-hardening cementitious composites (PVA-SHCC). Constr Build Mater 197:107–116
30. Sarwar MS, Niazi MBK, Jahan Z, Ahmad T, Hussain A (2018) Preparation and characterization of PVA/nanocellulose/Ag nanocomposite films for antimicrobial food packaging. Carbohyd Polym 184:453–464
31. Kim DS, Park HB, Rhim JW, Lee YM (2004) Preparation and characterization of crosslinked PVA/SiO2 hybrid membranes containing sulfonic acid groups for direct methanol fuel cell applications. J Membr Sci 240(1–2):37–48
32. Kamoun EA, Kenawy E-RS, Chen X (2017) A review on polymeric hydrogel membranes for wound dressing applications: PVA-based hydrogel dressings. J Adv Res 8(3):217–233
33. Zou G-X, Jin P-Q, Xin L-Z (2008) Extruded starch/PVA composites: water resistance, thermal properties, and morphology. J Elastomers Plast 40(4):303–316
34. Singh B, Sharma S, Dhiman A (2013) Design of antibiotic containing hydrogel wound dressings: biomedical properties and histological study of wound healing. Int J Pharm 457(1):82–91
35. Tian H, Yan J, Rajulu AV, Xiang A, Luo X (2017) Fabrication and properties of polyvinyl alcohol/starch blend films: effect of composition and humidity. Int J Biol Macromol 96:518–523
36. Ramaraj B (2007) Crosslinked poly (vinyl alcohol) and starch composite films. II. Physicomechanical, thermal properties and swelling studies. J Appl Polym Sci 103(2):909–916
37. Zhai M, Yoshii F, Kume T, Hashim K (2002) Syntheses of PVA/starch grafted hydrogels by irradiation. Carbohyd Polym 50(3):295–303
38. Tanpichai S, Oksman K (2016) Cross-linked nanocomposite hydrogels based on cellulose nanocrystals and PVA: mechanical properties and creep recovery. Composites A 88:226–233
39. Park S-N, Park J-C, Kim HO, Song MJ, Suh H (2002) Characterization of porous collagen/hyaluronic acid scaffold modified by 1-ethyl-3-(3-dimethylaminopropyl) carbodiimide cross-linking. Biomaterials 23(4):1205–1212
40. Chen J, Li Y, Zhang Y, Zhu Y (2015) Preparation and characterization of graphene oxide reinforced PVA film with boric acid as crosslinker. J Appl Polym Sci. https://doi.org/10.1002/app.42000
41. Hasanah A, Muhtadi A, Elyani I, Musfiroh I (2015) Epichlorohydrin as crosslinking agent for synthesis of carboxymethyl cellulose sodium (Na-CMC) as pharmaceutical excipient from water hyacinth (*Eichorrnia crassipes* L.). Int J Chem Sci 13(3):1227–1237
42. Bigi A, Cojazzi G, Panzavolta S, Roveri N, Rubini K (2002) Stabilization of gelatin films by crosslinking with genipin. Biomaterials 23(24):4827–4832
43. Destaye AG, Lin C-K, Lee C-K (2013) Glutaraldehyde vapor cross-linked nanofibrous PVA mat with in situ formed silver nanoparticles. ACS Appl Mater Interfaces 5(11):4745–4752
44. Vieira MGA, da Silva MA, dos Santos LO, Beppu MM (2011) Natural-based plasticizers and biopolymer films: a review. Eur Polym J 47(3):254–263
45. Sejidov FT, Mansoori Y, Goodarzi N (2005) Esterification reaction using solid heterogeneous acid catalysts under solvent-less condition. J Mol Catal A 240(1–2):186–190
46. Kaur K, Jindal R, Maiti M, Mahajan S (2019) Studies on the properties and biodegradability of PVA/Trapa natans starch (N-st) composite films and PVA/N-st-g-poly (EMA) composite films. Int J Biol Macromol 123:826–836
47. Labbez C, Fievet P, Szymczyk A, Vidonne A, Foissy A, Pagetti J (2002) Analysis of the salt retention of a titania membrane using the "DSPM" model: effect of pH, salt concentration and nature. J Membr Sci 208(1–2):315–329
48. Wang J, Li M, Zhou S, Xue A, Zhang Y, Zhao Y, Zhong J, Zhang Q (2017) Graphitic carbon nitride nanosheets embedded in poly (vinyl alcohol) nanocomposite membranes for ethanol dehydration via pervaporation. Sep Purif Technol 188:24–37
49. Moermans B, De Beuckelaer W, Vankelecom IF, Ravishankar R, Martens JA, Jacobs PA (2000) Incorporation of nano-sized zeolites in membranes. Chem Commun 24:2467–2468
50. Zhao C, Jiang Z, Zhao J, Cao K, Zhang Q, Pan F (2014) High pervaporation dehydration performance of the composite membrane with an ultrathin alginate/poly (acrylic acid)–Fe3O4 active layer. Ind Eng Chem Res 53(4):1606–1616
51. Guo R, Ma X, Hu C, Jiang Z (2007) Novel PVA–silica nanocomposite membrane for pervaporative dehydration of ethylene glycol aqueous solution. Polymer 48(10):2939–2945
52. Feng C, Khulbe K, Matsuura T, Tabe S, Ismail A (2013) Preparation and characterization of electro-spun nanofiber membranes and their possible applications in water treatment. Sep Purif Technol 102:118–135
53. Zhang X, Xie X, Wang H, Zhang J, Pan B, Xie Y (2012) Enhanced photoresponsive ultrathin graphitic-phase C3N4 nanosheets for bioimaging. J Am Chem Soc 135(1):18–21
54. Hassan A, Niazi MBK, Hussain A, Farrukh S, Ahmad T (2018) Development of anti-bacterial pva/starch based hydrogel membrane for wound dressing. J Polym Environ 26(1):235–243
55. Reis EFd, Campos FS, Lage AP, Leite RC, Heneine LG, Vasconcelos WL, Lobato ZIP, Mansur HS (2006) Synthesis and characterization of poly (vinyl alcohol) hydrogels and hybrids for rMPB70 protein adsorption. Mater Res 9(2):185–191
56. Hou T, Guo K, Wang Z, Zhang X-F, Feng Y, He M, Yao J (2019) Glutaraldehyde and polyvinyl alcohol crosslinked cellulose membranes for efficient methyl orange and Congo red removal. Cellulose 26(8):5065–5074
57. He S, Wang J, Yu M, Xue Y, Hu J, Lin J (2019) Structure and mechanical performance of poly (vinyl alcohol) nanocomposite by incorporating graphitic carbon nitride nanosheets. Polymers 11(4):610
58. Kamoun EA, Youssef ME, Abu-Saied M, Fahmy A, Khalil HF, Abdelhai F (2015) Ion conducting nanocomposite membranes based on PVA-HA-HAP for fuel cell application: II. Effect of modifier agent of PVA on membrane properties. Int J Electrochem Sci 10:6627–6644
59. Ramachandran VS, Beaudoin JJ (2000) Handbook of analytical techniques in concrete science and technology: principles, techniques and applications. Elsevier, Amsterdam
60. Kamoun EA, Kenawy E-RS, Tamer TM, El-Meligy MA, Eldin MSM (2015) Poly (vinyl alcohol)-alginate physically crosslinked hydrogel membranes for wound dressing applications: characterization and bio-evaluation. Arab J Chem 8(1):38–47
61. Roy N, Saha N, Kitano T, Vitkova E, Saha P (2011) Effectiveness of polymer sheet layer to protect hydrogel dressings. In: Trends in Colloid and Interface Science XXIV. Springer, pp 127–130
62. Thangavel P, Ramachandran B, Kannan R, Muthuvijayan V (2017) Biomimetic hydrogel loaded with silk and l-proline for tissue engineering and wound healing applications. J Biomed Mater Res B 105(6):1401–1408
63. Yang J, Shi G, Bei J, Wang S, Cao Y, Shang Q, Yang G, Wang W (2002) Fabrication and surface modification of macroporous poly (L-lactic acid) and poly (L-lactic-co-glycolic acid)(70/30) cell scaffolds for human skin fibroblast cell culture. J Biomed Mater Res 62(3):438–446

64. Winkler LW (1888) The determination of dissolved oxygen in water. Berlin DeutChem Gas 21:2843–2855
65. Wang X, Maeda K, Thomas A, Takanabe K, Xin G, Carlsson JM, Domen K, Antonietti M (2009) A metal-free polymeric photocatalyst for hydrogen production from water under visible light. Nat Mater 8(1):76
66. Cao K, Jiang Z, Zhang X, Zhang Y, Zhao J, Xing R, Yang S, Gao C, Pan F (2015) Highly water-selective hybrid membrane by incorporating g-C3N4 nanosheets into polymer matrix. J Membr Sci 490:72–83
67. Wang J, Li M, Zhou S, Xue A, Zhang Y, Zhao Y, Zhong J (2018) Controllable construction of polymer/inorganic interface for poly (vinyl alcohol)/graphitic carbon nitride hybrid pervaporation membranes. Chem Eng Sci 181:237–250
68. Niu P, Zhang L, Liu G, Cheng HM (2012) Graphene-like carbon nitride nanosheets for improved photocatalytic activities. Adv Funct Mater 22(22):4763–4770
69. Lotsch BV, Döblinger M, Sehnert J, Seyfarth L, Senker J, Oeckler O, Schnick W (2007) Unmasking melon by a complementary approach employing electron diffraction, solid-state NMR spectroscopy, and theoretical calculations—structural characterization of a carbon nitride polymer. Chemistry 13(17):4969–4980
70. Alghezawi N, Şanlı O, Aras L, Asman G (2005) Separation of acetic acid–water mixtures through acrylonitrile grafted poly (vinyl alcohol) membranes by pervaporation. Chem Eng Process 44(1):51–58
71. Baghaie S, Khorasani MT, Zarrabi A, Moshtaghian J (2017) Wound healing properties of PVA/starch/chitosan hydrogel membranes with nano Zinc oxide as antibacterial wound dressing material. J Biomater Sci Polym Ed 28(18):2220–2241
72. Luo X, Li J, Lin X (2012) Effect of gelatinization and additives on morphology and thermal behavior of corn starch/PVA blend films. Carbohyd Polym 90(4):1595–1600
73. Li Y, He G, Wang S, Yu S, Pan F, Wu H, Jiang Z (2013) Recent advances in the fabrication of advanced composite membranes. J Mater Chem A 1(35):10058–10077
74. Zhao X, Zhang Q, Chen D, Lu P (2010) Enhanced mechanical properties of graphene-based poly (vinyl alcohol) composites. Macromolecules 43(5):2357–2363
75. Li J, Shao L, Yuan L, Wang Y (2014) A novel strategy for making poly (vinyl alcohol)/reduced graphite oxide nanocomposites by solvothermal reduction. Mater Des 1980–2015(54):520–525
76. Zhang L, Wang Z, Xu C, Li Y, Gao J, Wang W, Liu Y (2011) High strength graphene oxide/polyvinyl alcohol composite hydrogels. J Mater Chem 21(28):10399–10406
77. Fan L, Yang H, Yang J, Peng M, Hu J (2016) Preparation and characterization of chitosan/gelatin/PVA hydrogel for wound dressings. Carbohyd Polym 146:427–434
78. Yokoyama F, Masada I, Shimamura K, Ikawa T, Monobe K (1986) Morphology and structure of highly elastic poly (vinyl alcohol) hydrogel prepared by repeated freezing-and-melting. Colloid Polym Sci 264(7):595–601
79. Wang M, Li J, Li W, Du Z, Qin S (2018) Preparation and characterization of novel poly (vinyl alcohol)/collagen double-network hydrogels. Int J Biol Macromol 118:41–48
80. Pal K, Banthia A, Majumdar D (2006) Preparation of transparent starch based hydrogel membrane with potential application as wound dressing. Trends Biomater Artif Organs 20(1):59–67
81. Jaiswal M, Dinda AK, Gupta A, Koul V (2010) Polycaprolactone diacrylate crosslinked biodegradable semi-interpenetrating networks of polyacrylamide and gelatin for controlled drug delivery. Biomed Mater 5(6):065014
82. Winter GD (1962) Formation of the scab and the rate of epithelization of superficial wounds in the skin of the young domestic pig. Nature 193(4812):293
83. Huang Y, Wang P, Wang Z, Rao Y, Cao J-j, Pu S, Ho W, Lee SC (2019) Protonated g-C3N4/Ti3+ self-doped TiO2 nanocomposite films: Room-temperature preparation, hydrophilicity, and application for photocatalytic NOx removal. Appl Catal B 240:122–131
84. Parra D, Tadini C, Ponce P, Lugão A (2004) Mechanical properties and water vapor transmission in some blends of cassava starch edible films. Carbohyd Polym 58(4):475–481
85. Vrana N, O'Grady A, Kay E, Cahill P, McGuinness G (2009) Cell encapsulation within PVA-based hydrogels via freeze-thawing: a one-step scaffold formation and cell storage technique. J Tissue Eng Regenerat Med 3(7):567–572
86. Qi X, Hu X, Wei W, Yu H, Li J, Zhang J, Dong W (2015) Investigation of Salecan/poly (vinyl alcohol) hydrogels prepared by freeze/thaw method. Carbohyd Polym 118:60–69
87. Yiamsawas D, Kangwansupamonkon W, Chailapakul O, Kiatkamjornwong S (2007) Synthesis and swelling properties of poly [acrylamide-co-(crotonic acid)] superabsorbents. React Funct Polym 67(10):865–882
88. Zhang D, Zhou W, Wei B, Wang X, Tang R, Nie J, Wang J (2015) Carboxyl-modified poly (vinyl alcohol)-crosslinked chitosan hydrogel films for potential wound dressing. Carbohyd Polym 125:189–199
89. Biranje SS, Madiwale PV, Patankar KC, Chhabra R, Dandekar-Jain P, Adivarekar RV (2019) Hemostasis and anti-necrotic activity of wound-healing dressing containing chitosan nanoparticles. Int J Biol Macromol 121:936–946
90. Qi XN, Mou ZL, Zhang J, Zhang ZQ (2014) Preparation of chitosan/silk fibroin/hydroxyapatite porous scaffold and its characteristics in comparison to bi-component scaffolds. J Biomed Mater Res A 102(2):366–372
91. Mehrabani MG, Karimian R, Mehramouz B, Rahimi M, Kafil HS (2018) Preparation of biocompatible and biodegradable silk fibroin/chitin/silver nanoparticles 3D scaffolds as a bandage for antimicrobial wound dressing. Int J Biol Macromol 114:961–971
92. El Fawal GF, Abu-Serie MM, Hassan MA, Elnouby MS (2018) Hydroxyethyl cellulose hydrogel for wound dressing: fabrication, characterization and in vitro evaluation. Int J Biol Macromol 111:649–659
93. Pourjavadi A, Nazari M, Hosseini SH (2015) Synthesis of magnetic graphene oxide-containing nanocomposite hydrogels for adsorption of crystal violet from aqueous solution. RSC Adv 5(41):32263–32271
94. Ninan N, Muthiah M, Park I-K, Elain A, Thomas S, Grohens Y (2013) Pectin/carboxymethyl cellulose/microfibrillated cellulose composite scaffolds for tissue engineering. Carbohyd Polym 98(1):877–885
95. Wittaya-areekul S, Prahsarn C (2006) Development and in vitro evaluation of chitosan–polysaccharides composite wound dressings. Int J Pharm 313(1–2):123–128
96. Riđanović L, Riđanović S, Jurica D, Spasojević P (2010) Evaluation of water temperature and dissolved oxygen regimes in River Neretva. BALWOIS Ohrid
97. Singh B, Pal L (2012) Sterculia crosslinked PVA and PVA-poly (AAm) hydrogel wound dressings for slow drug delivery: mechanical, mucoadhesive, biocompatible and permeability properties. J Mech Behav Biomed Mater 9:9–21

Affiliations

Arooj Ahmed[1] · Muhammad Bilal Khan Niazi[1] · Zaib Jahan[1] · Ghufrana Samin[2] · Erum Pervaiz[1] · Arshad Hussain[1] · Muhammad Taqi Mehran[1]

[1] Department of Chemical Engineering, School of Chemical and Materials Engineering, National University of Sciences and Technology, Islamabad, Pakistan

[2] Department of Chemistry, University of Engineering and Technology Lahore, Faisalabad Campus, Lahore, Pakistan